Linear stability of acoustic streaming flows in microchannels

A. Kwang-Hua Chu
P. O. Box 39, Tou-Di-Ban, Xihong Road, Urumqi 830000, People's Republic of China
(Received 13 December 2004; revised manuscript received 13 June 2005; published 22 December 2005)

We study the stability of acoustic streaming flows of fluids induced by a small-amplitude surface acoustic wave propagating along the walls of a confined parallel-plane microchannel or microslab in the incompressible flow regime. The secondary (Navier) slip flows are of negligible effect on the stability characteristic compared with the primary (Navier) slip flow. The governing equation, which was derived by considering the weakly nonlinear coupling between the wavy interface and the viscous fluid, is obtained by taking into account the (Navier) slip conditions and then the eigenvalue problem is solved by a verified numerical code together with the associated dynamic and kinematic conditions. The value of the critical Reynolds number was found to be near 1441 which is smaller than the value 5772 for conventional pressure-driven flows.

DOI: 10.1103/PhysRevE.72.066311 PACS number(s): 47.20.Ma, 02.30.Mv, 68.08.−p

I. INTRODUCTION

Both high and low frequency surface acoustic waves (SAWs) are interesting and important subjects in physics as well as in many other scientific applications [1–3]. One example is the characterization of physical and chemical properties of complicated materials. Relevant problems are the instability of the flow induced by a SAW and the slip effect existing along the interface of a quantum fluid [4–6]. In fact, the instability may trigger the laminar-turbulent transition for flows of a superfluid. The important issue is to determine the critical velocity [6] for the relevant physical parameters so that the experimental measurements can be under control.

An other example is related to the possibility of pumping molecules and atoms near or along surfaces under the perturbing influence of a SAW [4,5,7]. In fact, with the latter, it has been reported that people can make microflow systems that could circulate heat-transfer fluids over silicon chips, reconstitute dried drugs, and possibly synthesize chemicals from liquid and solid constituents [7], although the flow control for this system is still in progress and the understanding of the flow stability is rather limited up to now. We also note that acoustic or steady streaming flow, or the mean flow induced by boundaries, has been intensively studied since the late 1800s [8–11]. Preliminary theoretical results in the free molecular regime showed some disagreement with other approaches [4,5,12].

For quantum fluids or liquids in microdomains, however, there always exists a slip velocity along the static interface or confinement due to the microscopically incomplete momentum exchange therein [13–15]. The distinction among various flow regimes can be obtained by introducing the Knudsen number (Kn), which can also characterize the value of the slip velocity [13,14] or the Navier slip parameter $N_s = \mu S/d$. This is dimensionless; S is the proportionality constant in $u_s = S\tau$, where τ is the shear stress of the bulk velocity, and u_s is the dimensional slip velocity. For the no-slip case, $S=0$, but for a no-stress condition $S=\infty$. μ is the fluid viscosity and d is one-half of the channel width [15]. Kn $=$mfp$/L$, where mfp is the mean free path of the fluid and L is the characteristic flow dimension. Slip flow conditions exist for $0.001 < \mathrm{Kn} \leqslant 0.1$, where the flow can be considered continuous if the slip velocity at the walls is taken into account. Nonzero slip velocity is due to incomplete momentum and energy exchange between the colliding fluid particles and the solid boundaries.

Meanwhile, the effect of elastic or deformable interfaces, like surface acoustic waves, interacting with bulk and surface phonons (propagating along the elastic boundaries [16–18]) upon the stability of slip flows, has seldom been considered before, to the best knowledge of the authors. Although mathematical difficulty is essential therein, we have performed a preliminary study of the linear stability of acoustic streaming flows in a plane channel without considering the slip effect along the interface or wall [19]. In this work, the stability analysis of incompressible slip flows for normal fluids inside a microchannel with the flow confined by two elastic (wall) layers of thin films, where surface acoustic waves are propagating along the interfaces, is conducted. That is, we relax the static or rigid-interface boundary conditions which are frequently used in previous theoretical and/or experimental approaches to dynamic or deformable-interface boundary conditions, which are more realistic in essence especially when we consider the flow stability problem in a microdomain where surface acoustic waves propagate along the elastic boundaries. A verified code based on the spectral method developed by Chu [19] will be extended here to include the boundary conditions coming from SAWs existing along the interfaces to obtain the stability characteristics of the basic slip flow.

This paper is organized as follows. We introduce the mathematical formulation for the physical problems we shall investigate by using the Orr-Sommerfeld equation and then the relevant linear stability analysis in Sec. II. The coordinate system and relevant notations will be described first. The fundamental governing equation and definition of physical but dimensionless parameters then follow. Boundary conditions for the slip flow and the wavy interface of the fluid system are then incorporated. We shall investigate the expression for primary slip flows of fluids and their stability characteristic will be derived before we describe the numerical approach, a modified spectral method at the end of this section. Two physical parameters K_0 [relevant to the acoustic streaming or wavy interface (due to the SAWs) effect] and

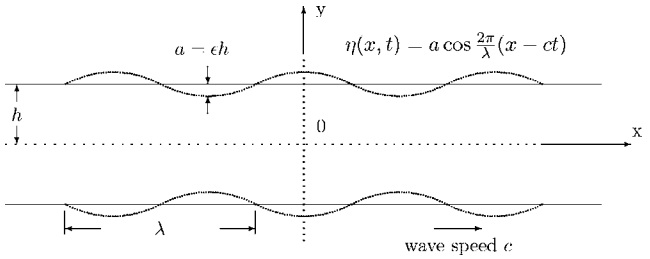

FIG. 1. Schematic diagram of the wavy motion of the flexible walls of a microchannel.

Kn will be introduced or defined. Finally we shall present our calculations and discuss them. Our results illustrate that the critical Reynolds number (Re_{cr}) decreases (to 1441) rapidly once the interfaces are subjected to propagating waves (or noises) and there are slip velocities existing along the boundaries or interfaces ($K_0=1$ and $\mathrm{Kn}=0.001$). However, the slip velocity (adjusted by Kn) effect is minor and adverse compared to the acoustic streaming or wavy interface effect (tuned by K_0) when considering the decrease of Re_{cr}.

II. FORMULATIONS

We note that entrainment of fluids induced by SAWs propagating along deformable boundaries has been studied [4,5,16] since the early 1950s. The role of elastic macroscopic walls resembles that of microscopic phonons [5]. To escape from the above mentioned difficulties (microscopic many-body problems), we plan to use a macroscopic approach which is a complicated extension of previous approaches [19,20].

A. Physical interface treatment

We consider a two-dimensional layer (slab) of uniform thickness filled with a homogeneous normal fluid (Newtonian viscous fluid; its dynamics is described by Navier-Stokes equations). The upper and lower boundaries of the layer are interfaces which are rather flexible, on which are imposed traveling sinusoidal waves of small amplitude a (due to SAWs or peristaltic waves). The vertical displacements of the upper and lower interfaces ($y=h$ and $-h$) are thus presumed to be η and $-\eta$, respectively, where $\eta=a\cos(2\pi/\lambda)\times(x-ct)$, λ is the wavelength, and c the wave speed. x and y are Cartesian coordinates, with x measured in the direction of wave propagation and y measured in the direction normal to the mean position of the interfaces. The schematic plot is illustrated in Fig. 1. It is expedient to simplify these equations by introducing dimensionless variables. We have a characteristic velocity c and three characteristic lengths a, λ, and h. The following variables based on c and h can thus be introduced:

$$x' = \frac{x}{h}, \quad y' = \frac{y}{h}, \quad u' = \frac{u}{c}, \quad v' = \frac{v}{c}, \quad \eta' = \frac{\eta}{h},$$

$$\psi' = \frac{\psi}{ch}, \quad t' = \frac{ct}{h}, \quad p' = \frac{p}{\rho c^2},$$

where ψ is the dimensional stream function, and ρ and p are the density and pressure of the fluid, respectively. After introducing the dimensionless variables, now, for the ease and direct representation of our mathematical expressions in the following, we shall drop the primes on those dimensionless variables. The relevant governing equations for an incompressible flow are

$$\boldsymbol{\nabla}\cdot\mathbf{u}=0 \quad \text{or} \quad \partial u/\partial x + \partial v/\partial y = 0, \quad \mathbf{u}\equiv(u,v);$$

$$\partial\mathbf{u}/\partial t + \mathbf{u}\cdot\boldsymbol{\nabla}\mathbf{u} = -\boldsymbol{\nabla}p + \nabla^2\mathbf{u}/\mathrm{Re},$$

with $u=\partial\psi/\partial y$, $v=-\partial\psi/\partial x$. $\mathrm{Re}=\rho u_0 h/\mu$ is the Reynolds number with ρ and μ being the density and viscosity of the fluid. u_0 is the characteristic velocity in the physical domain. For our interest here, the amplitude ratio ϵ, the wave number α, and the Reynolds number Re_{sw} are defined by

$$\epsilon = \frac{a}{h}, \quad \alpha = \frac{2\pi h}{\lambda}, \quad \mathrm{Re}_{sw} = \frac{ch}{\nu}.$$

Note that the Reynolds number Re_{sw}, which is based on the phase speed of the surface wave, is much larger than the Reynolds number Re, which is based on the maximum speed of the fluid flow in microchannels.

To derive the linearized equations by taking into account the wavy-interface effect, we seek a solution in the form of a series in the parameter $\epsilon(\epsilon\ll 1)$:

$$\psi = \psi_0 + \epsilon\psi_1 + \epsilon^2\psi_2 + \cdots,$$

$$\frac{\partial p}{\partial x} = \left(\frac{\partial p}{\partial x}\right)_0 + \epsilon\left(\frac{\partial p}{\partial x}\right)_1 + \epsilon^2\left(\frac{\partial p}{\partial x}\right)_2 + \cdots.$$

The two-dimensional (x and y) momentum equations and the equation of continuity for the normal fluid can be in terms of the stream function ψ if the pressure (p) term is eliminated. The final governing equation is

$$\frac{\partial}{\partial t}\nabla^2\psi + \psi_y\nabla^2\psi_x - \psi_x\nabla^2\psi_y = \frac{1}{\mathrm{Re}_{sw}}\nabla^4\psi, \quad \nabla^2 \equiv \frac{\partial^2}{\partial x^2} + \frac{\partial^2}{\partial y^2}, \tag{1}$$

and subscripts indicate partial differentiation. We presume originally that the fluid is quiescent (this corresponds to the free pumping case) and finally the velocity profile of the fluid is symmetric with respect to the centerline of the plane channel bounded by the elastic interfaces. The fluid is subjected to boundary conditions imposed by the symmetric motion of the walls and the nonzero velocity slip: $u = \mp\,\mathrm{Kn}\,du/dy$ [14,15], $v=\pm\partial\eta/\partial t$ at $y=\pm(1+\eta)$; here $\mathrm{Kn}=\mathrm{mfp}/h$. The boundary conditions may be expanded in powers of η and then ϵ:

$$\psi_{0y1} + \epsilon[\cos\alpha(x-t)\psi_{0yy}|_1 + \psi_{1y}|_1] + \epsilon^2\left(\frac{\psi_{0yyy}|_1}{2}\cos^2\alpha(x-t) + \psi_{2y}|_1 + \cos\alpha(x-t)\psi_{1yy}|_1\right) + \cdots$$

$$= -\mathrm{Kn}\left[\psi_{0yy}|_1 + \epsilon[\cos\alpha(x-t)\psi_{0yyy}|_1 + \psi_{1yy}|_1] + \epsilon^2\left(\frac{\psi_{0yyyy}|_1}{2}\cos^2\alpha(x-t) + \cos\alpha(x-t)\psi_{1yyy}|_1 + \psi_{2yy}|_1\right) + \cdots\right], \psi_{0x}|_1$$

$$+ \epsilon[\cos\alpha(x-t)\psi_{0xy}|_1 + \psi_{1x}|_1] + \epsilon^2\left(\frac{\psi_{0xyy}|_1}{2}\cos^2\alpha(x-t) + \cos\alpha(x-t)\psi_{1xy}|_1 + \psi_{2x}|_1\right) + \cdots = -\epsilon\alpha\sin\alpha(x-t).$$

The equations above, together with the condition of symmetry and a uniform constant pressure gradient in the x direction, $(\partial p/\partial x)_0 = \text{const}$, yield

$$\psi_0 = K_0\left((1+2\mathrm{Kn})y - \frac{y^3}{3}\right), \quad K_0 = \frac{\mathrm{Re}_{sw}}{2}\left(-\frac{\partial p}{\partial x}\right)_0. \quad (2)$$

K_0 is in fact the necessary pumping to sustain a plane Poiseuille flow (pressure-driven case). ψ_0 corresponds to the solution of

$$\frac{\partial}{\partial t}\nabla^2\psi_0 + \psi_{0y}\nabla^2\psi_{0x} - \psi_{0x}\nabla^2\psi_{0y} = \frac{1}{\mathrm{Re}_{sw}}\nabla^4\psi_0, \quad (3)$$

together with above mentioned boundary conditions (for ψ_0). Note that

$$\psi_1 = \frac{1}{2}[\phi(y)e^{i\alpha(x-t)} + \phi^*(y)e^{-i\alpha(x-t)}], \quad (4)$$

where the asterisk denotes the complex conjugate. Substitution of ψ_1 into Eq. (1) yields

$$\left(\frac{d^2}{dy^2} - \alpha^2 + i\alpha\,\mathrm{Re}_{sw}[1 - K_0(1-y^2+2\mathrm{Kn})]\right)\left(\frac{d^2}{dy^2} - \alpha^2\right)\phi$$
$$- 2i\alpha K_0\,\mathrm{Re}_{sw}\phi = 0.$$

The normal fluid is subjected to boundary conditions imposed by the symmetric motion of the wavy interfaces and the slip condition at the interfaces. The basic slip flow now has this form, as $u = \partial\psi_0/\partial y$,

$$\bar{u} = K_0(1 - y^2 + 2\mathrm{Kn}), \quad (5)$$

where $\mathrm{Kn} = \mathrm{mfp}/h$. The boundary conditions become, for $-1 \leqslant y \leqslant 1$,

$$\phi_y(\pm 1) \pm \phi_{yy}(\pm 1)\mathrm{Kn} = 2K_0(1 \pm \mathrm{Kn}), \quad \phi(\pm 1) = \pm 1. \quad (6)$$

B. Governing equation for stability analysis

To obtain the stability characteristics for the above mentioned flows, we shall introduce the conventional Orr-Sommerfeld equation just for comparison and similar application. Macroscopically, the motion of a normal fluid (above the critical phase transition temperature of the quantum fluid) as a whole can be treated by using hydrodynamical models starting from the microscopic atomic wave function [21]. Here, after simplifying treatment of the complicated mathematical derivations, the dimensionless equations of motion for an incompressible normal fluid flow [19,20], in the absence of body forces and moments, reduce to

$$\frac{\partial \mathbf{U}}{\partial t} + (\mathbf{U}\cdot\boldsymbol{\nabla})\mathbf{U} = -\boldsymbol{\nabla}P + \frac{1}{\mathrm{Re}}\nabla^2\mathbf{U}, \quad (7)$$

where $\mathbf{U}$ and P stand for the velocity and pressure of the fluid [22]. $\mathrm{Re} = \rho u_{max} h/\mu$ is the Reynolds number. For the case of normal fluid flows driven by a constant pressure gradient, i.e., plane Poiseuille flow, the length scale is the half-width of the normal-fluid layer h, and the velocity is the centerline velocity u_{max}. Following the usual assumptions of linearized stability theory [22], $U_i(x_i,t) = \bar{u}_i(x_i) + u_i'(x_i,t)$, and similarly, $P(x_i,t) = \bar{p}(x_i) + p'(x_i,t)$, the linearized equation that governs the disturbances is

$$\frac{\partial u_i'}{\partial t} + (\bar{\mathbf{u}}\cdot\boldsymbol{\nabla})u_i' + (\mathbf{u}'\cdot\boldsymbol{\nabla})\bar{u}_i = -\boldsymbol{\nabla}p' + \frac{1}{\mathrm{Re}}\nabla^2 u_i'. \quad (8)$$

Disregarding the lateral disturbances, $w' = 0$, a stream function for the disturbance, ψ, can be defined such that $u' = \partial\psi/\partial y$, $v' = -\partial\psi/\partial x$. Using normal mode decomposition analysis, ψ may be assumed to have the form $\psi(x,y,t) = \phi(y)\exp[i\alpha(x - Ct)]$, where α is the wave number (real), and C is $C_r + iC_i$. This is a kind of Tollmien-Schlichting (TS) transversal wave. C_r is the ratio between the velocity of propagation of the wave of perturbation and the characteristic velocity, C_i is called the amplification factor, and α equals $2\pi\Lambda^{-1}$, where Λ is the wavelength of the TS perturbation [22]. Substituting the stream function and eliminating the pressure, we have the linearized disturbance equation

$$(D^2 - \alpha^2)(D^2 - \alpha^2)\phi = i\alpha\,\mathrm{Re}[(\bar{u} - C)(D^2 - \alpha^2)\phi - (D^2\bar{u})\phi], \quad (9)$$

where $D = d/dy$. This is also valid for the slip flow regime, $0.001 < \mathrm{Kn} \leqslant 0.1$, since the flow can still be considered as continuous. Note that this equation resembles that derived from ψ_1 after substituting ψ_1 into Eq. (1) [19] with suitable selections for ϕ, c, K_0, and the transformed Reynolds number Re. For slip flow, continuous models can be used if the no-slip boundary condition is modified. A few models have been suggested to estimate the nonzero velocity at a boundary surface [13–15]. In this study, we adopt the approach based on Taylor's expansion of the velocity around the wall. Thus, the first order approximation yields $\bar{u}|_{wall} = \mathrm{Kn}\,d\bar{u}/dy$

(positive for the inner normal as $y \equiv n$). Consequently, the mean (basic) velocity profile is given by

$$\bar{u} = 1 - y^2 + 2\mathrm{Kn} \tag{10}$$

for $-1 \leqslant y \leqslant 1$ [14]. The boundary conditions for ϕ or $D\phi$ are not the same as in the previous no-slip approach, i.e., $\phi(\pm 1) = D\phi(\pm 1) = 0$ [20], and have been introduced above [see Eq. (6)]. In fact, the Navier slip parameter (N_s) [15] can also play the role of the Knudsen number in the representation of the slip velocity (with $N_s \equiv \mathrm{Kn}$, especially when we consider the liquid flow).

C. Numerical approach

The eigenvalue problem raised above can be solved by using a verified code [19], which used the spectral method [20,23] based on the Chebyshev polynomial expansion approach, once the equation and boundary conditions are discretized. For instance, we have, from Eq. (3), as a finite-sum approximation (reduction from ∞ to N),

$$\phi(z) = \sum_{n=0}^{N} a_n T_n(z),$$

where $T_n(z)$ is the Chebyshev polynomial [20,23] of degree n with $z = \cos(\theta)$. $T_n(z)$ are known to satisfy the recurrence relations

$$zT_n(z) = \frac{1}{2}[T_{n+1}(z) + T_{n-1}(z)].$$

After substituting ϕ into Eq. (3) and with tremendous manipulations, we obtain the algebraic equation

$$\begin{aligned}
&\frac{1}{24} \sum_{\substack{p=n+4 \\ p \equiv n (\mathrm{mod}\ 2)}}^{N} [p^3(p^2-4)^2 - 3n^2p^5 + 3n^4p^3 - pn^2(n^2-4)^2]a_p \\
&- \sum_{\substack{p=n+2 \\ p \equiv n (\mathrm{mod}\ 2)}}^{N} \Bigg[\Bigg(2\alpha^2 + \frac{1}{4} i\alpha\, \mathrm{Re}(4M_0 f - 4C - M_0 c_n \\
&- M_0 c_{n-1}) \Bigg) p(p^2 - n^2) - \frac{1}{4} i\alpha\, \mathrm{Re}\, M_0 c_n p\big(p^2 - (n+2)^2\big)^2 \Bigg] \\
&- \frac{1}{4} i\alpha\, \mathrm{Re}\, M_0 d_{n-2} p[p^2 - (n-2)^2) \Bigg] a_p + i\alpha\, \mathrm{Re}\, M_0 n \\
&\times (n-1)a_n + \{\alpha^4 + i\alpha\, \mathrm{Re}[(M_0 f - C)\alpha^2 - 2M_0]\} c_n a_n \\
&- \frac{1}{4} i\alpha^3\, \mathrm{Re}\, M_0 [c_{n-2}a_{n-2} + c_n(c_n + c_{n-1})a_n + c_n a_{n+2}] = 0
\end{aligned} \tag{11}$$

for $n \geqslant 0$, $f = 1 + 2\mathrm{Kn}$, where $c_n = 0$ if $n > 0$, and $d_n = 0$ if $n < 0$, $d_n = 1$ if $n \geqslant 0$. Here, $M_0 = 1$, and C is the complex eigenvalue. The numerical boundary conditions [from Eq. (6)] become

$$\sum_{\substack{n=1 \\ n \equiv 1 (\mathrm{mod}\ 2)}}^{N} a_n = 1, \qquad \sum_{\substack{n=1 \\ n \equiv 1 (\mathrm{mod}\ 2)}}^{N} \left(n^2 + \mathrm{Kn}\frac{n^2(n^2-1)}{3} \right) a_n = 2K_0. \tag{12}$$

Equation (12) is different from that used in the no-slip treatment [19] mainly because of the (Navier) slip parameter being nonzero here. The complexities can be understood by recalling Eq. (6): ϕ_{yy} appears (second-order derivative of ϕ) once Kn is not zero. This term is not trivial when using the spectral method for the Chebyshev polynomial expansion (cf. Refs. [20,23]). It means the treatment of matrices thus formed becomes much more complicated than before.

The matrices thus formed are of poor condition because they are not diagonal and symmetric. Thus, before we perform floating-point computations to get the complex eigenvalues, we precondition these complex matrices to get less errors. Here we adapt Osborne's algorithm [24] to precondition these complex matrices via rescaling, i.e., by certain diagonal similarity transformations of the matrix (errors are in terms of the Euclidean norm of the matrix) designed to reduce its norm. The details of this algorithm can be traced in [24]. The form of the reduced matrix is upper Hessenberg. Finally we perform stabilized *LR* transformations for these matrices to get the complex eigenvalues (please see also [25] for the details). The preliminary verified results of this numerical code were obtained for the cases of Kn=0 (no-slip boundary conditions) in comparison with the benchmark results of Orszag [20]. For example, for Re=10 1000.0, $\alpha = 1.0$ of the test case, plane Poiseuille flow, we obtained the same values 0.2371 5261 48$+i$0.003 739 67 for $C_r + iC_i$ that Orszag obtained in 1971 [19,20].

III. RESULTS AND DISCUSSION

We first verify the no-slip results of this numerical code by calculating the critical Reynolds number for cases of no-slip boundary conditions in comparison with the benchmark results of Orszag [20]. For example, we obtain the same critical Reynolds number ($\mathrm{Re}_{cr} \sim 5772.2$) for the test case, plane Poiseuille flow, that Orszag obtained from CDC 7600 in 1971 [20]. After this, the subsequent numerical searching for Re_{cr} and corresponding α for our interest ($K_0 \neq 0$, effects of the acoustic streaming and interface; $\mathrm{Kn} \neq 0$, slip flow effects) is time consuming and variable.

To demonstrate some of the calculated spectra (C_r, C_i) near the regime of $(\mathrm{Re}_{cr}, \alpha)$, we plot Fig. 2 by selecting two pairs of $(\mathrm{Re}, \alpha) = (1562, 1.156)$ and $(2982.3, 1.0783)$ with the corresponding $K_0 = 1$ and 0.5 for the same Knudsen number (Kn=0.01). Once $C_i > 0$, instability occurs. The onset of instability occurs easily once the Reynolds number, wave number, or Knudsen number is perturbed a little near this regime (C_i becomes zero and then positive). To check the small amplitude effects (ϵ), we already calculated those spectra for $\epsilon = 0.01$ and found rather minor differences compared to the slip (Kn) and acoustic wave (K_0) effects.

We then plot the neutral stability boundary curves for different cases in Fig. 3. It is clear that each curve is composed

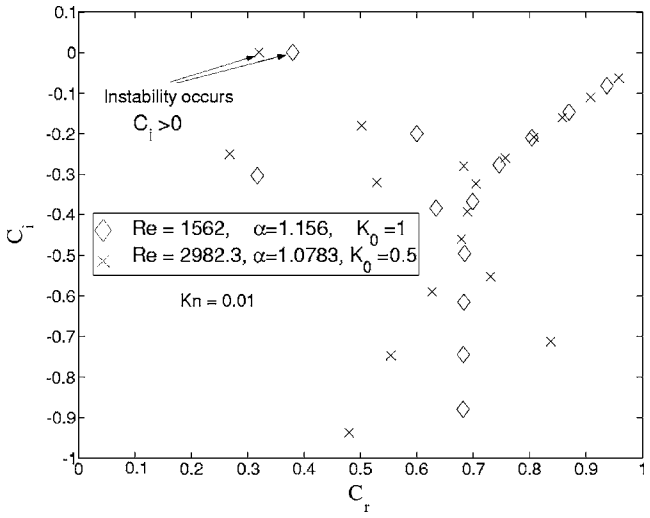

FIG. 2. Illustration of the temporal spectra (C_r, C_i) for disturbance waves due to acoustic streaming or interface (K_0) and slip velocity (Kn=0.01) effects. Re=1562, 2982.3 for corresponding $K_0=1$, 0.5 and $\alpha=1.156$, 1.0783, respectively.

of two branches [upper and lower; they coalesce into a critical point (Re_{cr} and α_{cr}) as the Reynolds number decreases]. We tune the K_0 parameter to be 1 and 0.5, with the corresponding Knudsen number being 0.001 and 0.01, respectively. Once the Knudsen number is set to be zero and there is no SAW effect, we recover the curve obtained by Orszag [20] ($\mathrm{Re}_{cr} \sim 5772$). Otherwise, the resulting critical Reynolds numbers (Re_{cr}) are 1441, 1562, 2664, and 2982.3, respectively. It seems the effect of SAWs propagating along the interface is the dominant one and will degrade the flow stability significantly. The slip velocity effect is minor and adverse (it delays the transition).

To understand the stability behavior related to the decay or amplification of the perturbed disturbance waves in a finite time for a certain mode, we also illustrate their time evolution patterns by selecting the least unstable mode. As illustrated in Figs. 4 and 5 for Re=1441, $\alpha=1.175$ $(K_0=1)$ and Re=2664, $\alpha=1.105$ $(K_0=0.5)$, we can observe an oscillating or amplifying pattern after a finite time (time is dimensionless and the Knudsen number is the same, Kn=0.001). The original disturbance (wave) will not decay for these unstable modes $(C_r, C_i) \sim (0.382, 0.000\,002)$ and $\sim(0.324, 0.000\,000\,46)$, respectively. Here, the amplitude ϕ is obtained by summing those contributions from finite modes (a_n) obtained from Eq. (11) and the corresponding (C_r, C_i). We remind the readers that the behavior at the near-wall and centerline regions shows different trends, which might be due to the wavy-interface effect.

To conclude in brief, we have observed that the instability of slip flow due to acoustic streaming in plane microchannels occurs very early, which is not favorable for the flow control in most physical, chemical, and biological applications.

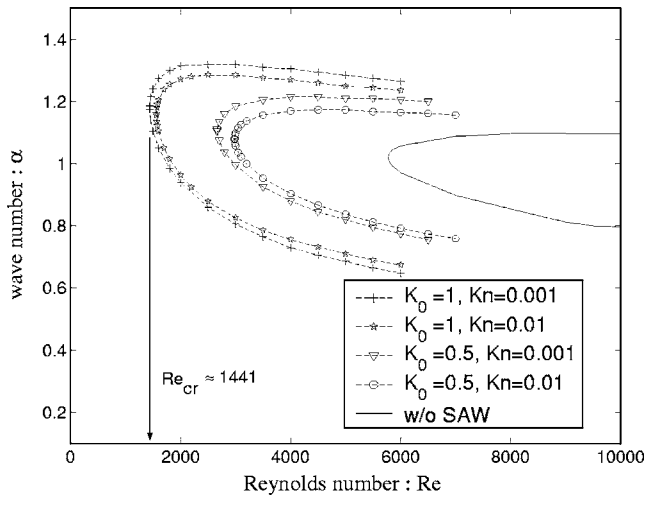

FIG. 3. Comparison of acoustic streaming or wavy interface (K_0) and slip velocity (Kn) effects on the neutral stability boundary of the basic flow. Kn=mfp/h. mfp is the mean free path of the quantum fluid. $\mathrm{Re}_{cr} \sim 1441$, 1562, 2664, 2982.3 for $K_0=1$, Kn =0.001, 0.01, and $K_0=0.5$, Kn=0.001, 0.01.

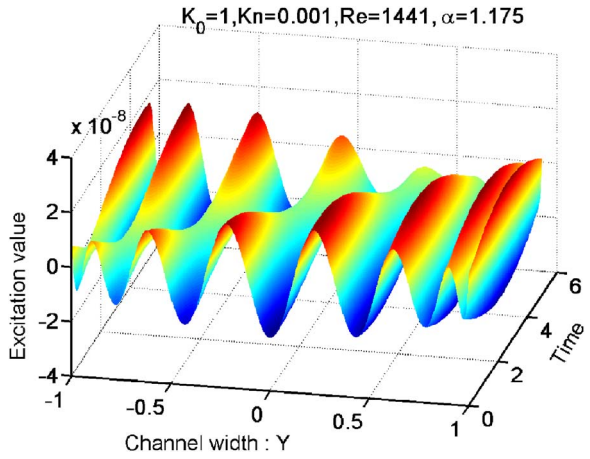

FIG. 4. (Color online) Illustration of the temporal evolution for disturbance waves due to interface (K_0) and slip velocity (Kn) effects. Re=1441 for corresponding $K_0=1$ and $\alpha=1.175$, Kn=0.001. Time is dimensionless.

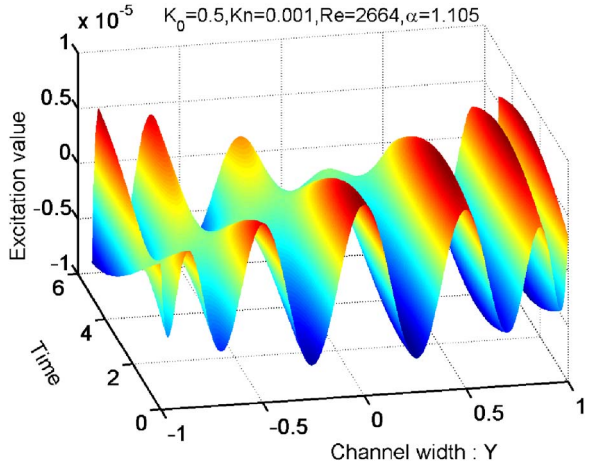

FIG. 5. (Color online) Illustration of the temporal evolution for disturbance waves due to interface (K_0) and slip velocity (Kn) effects. Re=2664 for corresponding $K_0=0.5$ and $\alpha=1.105$, Kn =0.001. Time is dimensionless.

Compared to the acoustic streaming effect (K_0), however, the slip effect (Kn) on the flow stability is only minor as evidenced in Fig. 3. This latter observation might be interpreted as due to the weakly nonlinear coupling between the elastic wall boundary and the inertia of the acoustic streaming flow. On the other hand, if we borrow an analogy from the slip of quantum fluids [13], we have also obtained more clues about the slip flow (which is in a nonequilibrium state) instability of quantum fluids (above their critical transition temperature) by considering more realistic interface conditions. Once we know the viscosities and/or densities of these quantum fluids, based on the obtained critical Reynolds number, we can then determine the critical velocity [6] for each case. Meanwhile, these results will help researchers to understand the formation or generation of vorticity waves [22] and then the route to low-temperature turbulence in quantum fluids [6]. We shall investigate more complicated relevant problems in the future [26]. For instance, ultrasound measurements play very important roles in ^{3}He investigation [2]. The time scale of ultrasound corresponds to quasiparticle lifetimes at low temperatures and first- to zero-sound crossover was observed. The energy scales of ultrasound match the binding energies of Cooper pairs in superfluid ^{3}He and coupling through density oscillations was observed. Sound transmission methods using many types of surface acoustic wave sensors have been developed for acoustical and electrical property measurements of adjacent liquid and gas (especially liquid ^{4}He at low temperature [3]). One example is that a Rayleigh SAW propagates along the substrate surface by emitting compressional waves into the quantum fluid and thus the sampling of the Rayleigh SAW is determined by the acoustic impedance of the surrounding quantum fluids.

ACKNOWLEDGMENT

This project is supported by the National Natural Science Foundation of China (NSFC) under Grant No. 10274061.

[1] R. L. Willett, Surf. Sci. **305**, 76 (1994); J. Freundenberg, M. von Schickfus, and S. Hunklinger, Sens. Actuators B **76**, 147 (2001); P. Hess, Phys. Today **55** (3), 42 (2002).
[2] W. P. Halperin and E. Varoquaux, in *Helium 3*, edited by W. P. Halperin and L. P. Pitaevskii (North-Holland, Amsterdam, 1990).
[3] Y. Aoki *et al.*, Physica B **329-333**, 234 (2003); K. Dransfeld and E. Salzmann, in *Physical Acoustics*, edited by W. P. Mason and R. N. Thurston (Academic Press, New York, 1970).
[4] P. Terry and M. W. P. Strandberg, J. Appl. Phys. **52**, 4281 (1981).
[5] V. D. Borman, S. Yu. Krylov, and A. M. Kharitonov, Sov. Phys. JETP **65**, 935 (1987).
[6] W. Zimmermann, Jr., Contemp. Phys. **37**, 219 (1996); V. P. Peshkov, in Proceedings of the Seventh International Conference or Low Temperature Physics, Toronto, 1960 (unpublished), p. 555; L. D. Landau and E. M. Lifshitz, *Fluid Mechanics*, 2nd ed. (Pergamon Press, New York, 1987).
[7] R. M. Moroney, R. M. White, and R. T. Howe, Appl. Phys. Lett. **59**, 774 (1991); N.-T. Nguyen, A. H. Meng, J. Black, and R. M. White, in *Proceedings of Transducers'99*, Sendai, 1999 (unpublished).
[8] O. Rudenko and S. Soluyan, *Theoretical Foundations of Nonlinear Acoustics* (Consultants Bureau, New York, 1977).
[9] W. L. Nyborg, in *Physical Acoustics*, edited by W. P. Mason (Academic Press, New York, 1965), Vol. 2, Pt. B, p. 265.
[10] W. Lauriks, L. Kelders, and J.-F. Allard, Wave Motion **18**, 59 (1998).
[11] M. Faraday, Philos. Trans. R. Soc. London **121**, 319 (1831).
[12] O. E. Aleksandrov, A. A. Elfimov, B. T. Porodnov, V. D. Seleznev, and A. G. Flyagin, Sov. Phys. Acoust. **35**, 561 (1989); K.-H. W. Chu, Eur. Phys. J.: Appl. Phys. **18**, 51 (2002).
[13] D. Einzel and J. M. Parpia, J. Low Temp. Phys. **109**, 1 (1997); A. Kundt and E. Warbung, Pogg. Ann. Phys. **156**, 177 (1875).
[14] M. N. Kogan, *Rarefied Gas Dynamics* (Plenum Press, New York, 1969).
[15] P. G. de Gennes, Langmuir **18**, 3013 (2002); C. L. M. Navier, C. R. Acad. Sci. Paris **6**, 389 (1827); A. K.-H. Chu, C. R. Mec. **332**, 895 (2004).
[16] M. S. Longuet-Higgins, Philos. Trans. R. Soc. London **345**, 535 (1953); A. K.-H. Chu, Electron. Lett. **38**, 1481 (2002).
[17] S. Mizuno, Physica B **316-317**, 230 (2002); P. Král and M. Shapiro, Phys. Rev. Lett. **86**, 131 (2001).
[18] A. Sergeev and V. Mitin, Physica B **316-317**, 276 (2002).
[19] A. K.-H. Chu, Phys. Rev. E **68**, 046305 (2003).
[20] S. A. Orszag, J. Fluid Mech. **50**, 689 (1971).
[21] R. P. Feynman, Phys. Rev. **94**, 262 (1954); I. M. Khalatnikov and V. V. Lebedev, J. Low Temp. Phys. **32**, 789 (1978); N. B. Kopnin, Rep. Prog. Phys. **65**, 1633 (2002).
[22] P. G. Drazin and W. H. Reid, *Hydrodynamic Stability* (Cambridge University Press, London, 1981); W. Heisenberg, Ann. Phys. **74**, 577 (1924); C. C. Lin, Q. Appl. Math. **4**, 277 (1946).
[23] D. Gottlieb and S. A. Orszag, *Numerical Analysis of Spectral Methods: Theory and Applications*, NSF-CBMS Monograph No. 26 (SIAM, Philadelphia, 1977).
[24] E. E. Osborne, J. Assoc. Comput. Mach. **7**, 338 (1960).
[25] J. H. Wilkinson, *The Algebraic Eigenvalue Problem* (Oxford University Press, Oxford, 1965); W. K.-H. Chu, J. Phys. A **34**, 3389 (2001).
[26] J. P. Wolfe, *Imaging Phonons: Acoustic Wave Propagation in Solids* (Cambridge University Press, Cambridge, 1998); G. A. Antonelli, P. Zannitto, and H. J. Maris, Physica B **317-317**, 377 (2002).